# First considerations for the design of the ESS cryo-modules

Aurélien Ponton*

EUROPEAN SPALLATION SOURCE

N° ESS-LD-TECHNOTE-0310AP

Linac Division *Technical Note*

**Abstract**

The ESS superconducting radio-frequency (SRF) linac aims at accelerating, focusing and ensuring the stability of proton beams from 50 $MeV$ up to 2.5 $GeV$. It is now well established that spoke resonators, thanks to their high accelerating efficiency and mechanical stability, are good candidates to cover the energy range from 50 $MeV$ up to 150 $MeV$. Elliptical cavities will then accelerate the beam up to 2.5 $GeV$. In order to give a first approximation of the linac dimension and to outline methods of cryostating, two different layouts have been investigated. Both of them are based on spoke and elliptic SRF cavities but with two different philosophies: either segmented design or not segmented design. These two approaches are presented and details of each layout are given in terms of lattice type, accelerating gradient or cryostat length and diameter. The study estimates the static and dynamic heat loads to provide a comparison of the two methods of cryostating.

*Contact: aurelien.ponton@esss.se

# Contents



# 1 Introduction

This note aims at maintaining the effort for the consolidation of the ESS linac architecture. Presenting segmented and not segmented schemes is in line with this global effort and should launch in-depth investigations.

In the two following studies, the proton beam is successively accelerated in one family of spoke resonators and two families of elliptical cavities. Spoke resonators work at $352.21\ MHz$ while elliptical cavities have a working frequency of $704.42\ MHz$. Because of a higher surface resistance and for mechanical stability reasons, the latter are maintained at $2\ K$ in sub-cooled liquid helium. Spoke resonators are generally supposed to work at $4.2\ K$. Nevertheless, operation at $2\ K$ may be considered since sufficient reduced RF losses at $2\ K$ could offset the financial aspect increase in refrigeration cost [6]. The last section compares $4.2\ K$ and $2\ K$ operations for the spoke section and gives an overall estimation of the total power consumption of the two linacs.

We present in section 5 the general layouts of the proposed linac architectures. We discuss also the relative induced differences when the design is based on full modularity on one hand and on cryo-strings on the other hand.

Section 4 is a review of the technological choices made for the ESS linac. It describes the accelerating cavity and focusing magnet parameters.

Cryostating is based on proven technologies developed at the SNS and by the Tesla collaboration for the XFEL and ILC. The key characteristics of both options are outlined in section 3.

# 2 Definitions

For the sake of clarity, it is mandatory to present the expression for the accelerating gradient $E_{acc}$ since no common definition is widely used in the accelerator community. In this note, the accelerating voltage $V_{acc}$ in a cavity is given, as a function of the reduced velocity $\beta$, by:

$$V_{acc}(\beta) = \left| \int E_z(r=0,z)\, e^{j\frac{\omega z}{\beta c}}\ \mathrm{d}z \right| \tag{1}$$

where:

- $E_z(r=0,z)$ is the longitudinal component of the electric field along the beam axis;
- $\omega$ is the angular frequency of the considered mode;
- $c$ is the speed of light in vacuum.

This voltage is normalized by an accelerating length $L_{acc}$ to give rise to:

$$E_{acc} = \frac{V_{acc}(\beta_{\text{opt}})}{L_{acc}} \tag{2}$$

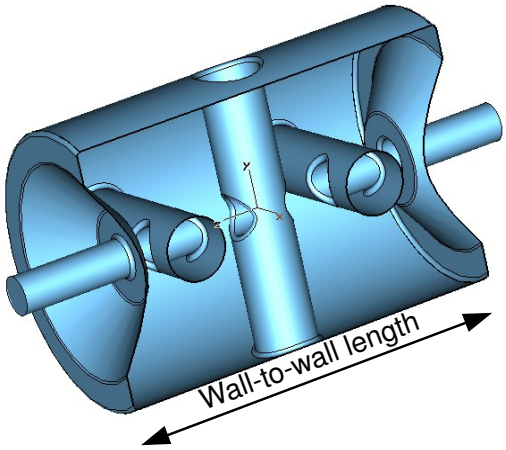


Figure 1: Definition of the wall-to-wall length in a triple-spoke cavity

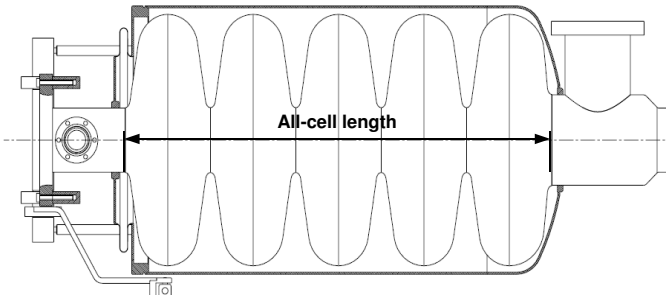


Figure 2: Definition of the all-cell length in a 5-cell-elliptical cavity

given at the optimal Beta $\beta_{\text{opt}}$ *i. e.* the Beta given the highest Transit Time Factor (TTF). For $L_{acc}$ we will use the expression (valid for $\pi$-mode):

$$L_{acc} = \frac{n_{\text{gap}}}{2}\beta_{\text{opt}}\lambda_{\text{RF}} \tag{3}$$

where $n_{\text{gap}}$ is the number of accelerating gaps and $\lambda_{\text{RF}}$ is the RF wavelength in vacuum of the resonator.
The definition of $L_{acc}$ in *Eq.* 3 has the advantage to compare the accelerating efficiency of cavities independently of their shape, frequency or energy range. This definition is used in the GenlinWin code [3] which has been used in this work.

Moreover, we will not deal with any geometrical Beta to refer to the physical length of a cavity. To avoid confusion, we will mention the "wall-to-wall" length for spoke resonators and "all-cell" length for the elliptical one's as defined on *Figs.* 1 and 2 respectively.

# 3 Presentation of the two methods for cryostating

This section gives a global description of the two cryostating options. It underlines the main goals of each method and their consequences on the cryo-module design.

## 3.1 Segmented design

The SRF linac of the SNS is based on a segmented design with 32 independent superconducting cryo-modules to raise the beam energy to $1.3\ GeV$ [13]. A cryo-module consists of a vacuum tank, a thermal shielding ($50\ K$) providing a radiation barrier between the cavities and the external world, a space frame and a string of cavities. The string is supported by four nitronic rods which limit the solid heat conduction to the cryogenic temperatures. These rods are also used to perform the cavity alignment process thanks to their special "X" pattern [19]. A schematic end view of an SNS medium-$\beta$ cryo-module is shown on *Fig.* 3. Between each cryo-module is a warm space ($1.6\ m$) containing the focusing quadrupole magnets, the diagnostics and the pumping system. These warm-to-cold transitions induce a significant increase to the total static losses (see section 6.1).

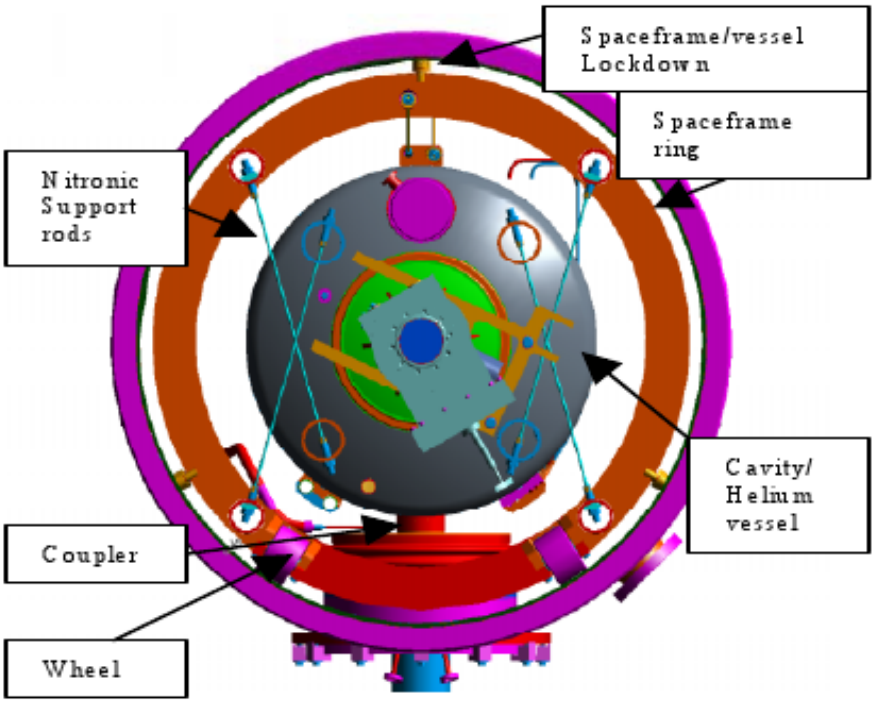


Figure 3: End view of an SNS medium-$\beta$ cryo-module [19]

From the vacuum and cryogenics point of view, each module is an independent unit. In order to feed the cavities with liquid helium, one cold box is needed for one cryo-module. It contains heat exchangers and Joule-Thomson valves for $2\ K$ operation. *The linac tunnel of the SNS including* $1.4\ m$ *diameter cryostats and valve boxes is* $3.8\ m$ *in height and* $4.3\ m$ *in width*.

The aim of the segmentation is to provide *a high reliability* with a low MTTR (Mean Time To Repair). At the SNS, the bayonet design for the connection of the helium line permits replacement of a cryo-module in less than one day.

We can notice that only elliptical cavities are taken into account in the SNS case. However, we can underline the fact that the EUROTRANS and the EURISOL have scheduled to use segmented cryo-modules not only for elliptical cavities but also for spoke resonators [2].

## 3.2 Not segmented design

The TESLA collaboration has extensively developed SRF technology which is now applied for the XFEL and ILC projects. Concerning cryo-modules, this work has led to a design based on cryo-strings [1]. A cryo-string consists of tens of connected cryo-modules. It is an independent unit from the cryogenics and vacuum point of view.

Designing cryo-strings aims at *minimizing the static heat load in the cryogenic section and maximizing the real-estate gradient*. The not segmented design objectives are achievable by reducing the warm-to-cold transitions and multiplying the thermal intercepts between the room temperature and the helium-cooled line. Magnets and diagnostics are consequently include into the cryo-module. In addition, the $2\ K$ components are surrounded by $5 - 8\ K$ intercepts for heat interception and radiation screening likewise surrounded by shielding in the temperature range from $50 - 80\ K$ as shown on *Fig.* 4.

The large Gas Return Pipe (in pink on *Fig.* 4) is the main support structure for the string of cavities and magnets. The alignment of the GRP is used to reference the axis of the active component. The helium distribution system needed to operate the cavities and magnets at $2\ K$ is integrated into the cryo-module. $2\ K$ helium is produced by one Joule-Thomson expansion valve per cryo-string. *The linac cylindrical shape tunnel is* $5.2\ m$ *in height for cryostats of about* $1\ m$ *in diameter* [1].

Due to the length of the XFEL and ILC main linacs ($1.7\ km$ and $30\ km$ respectively),

[1] Because of a higher working frequency ($1.3\ GHz$) the elliptical Tesla cavities are twice as smaller (at first order) as the elliptical ESS one's: a larger cryostat cross-section is then needed to accomodate the $704.42\ MHz$ cavities.

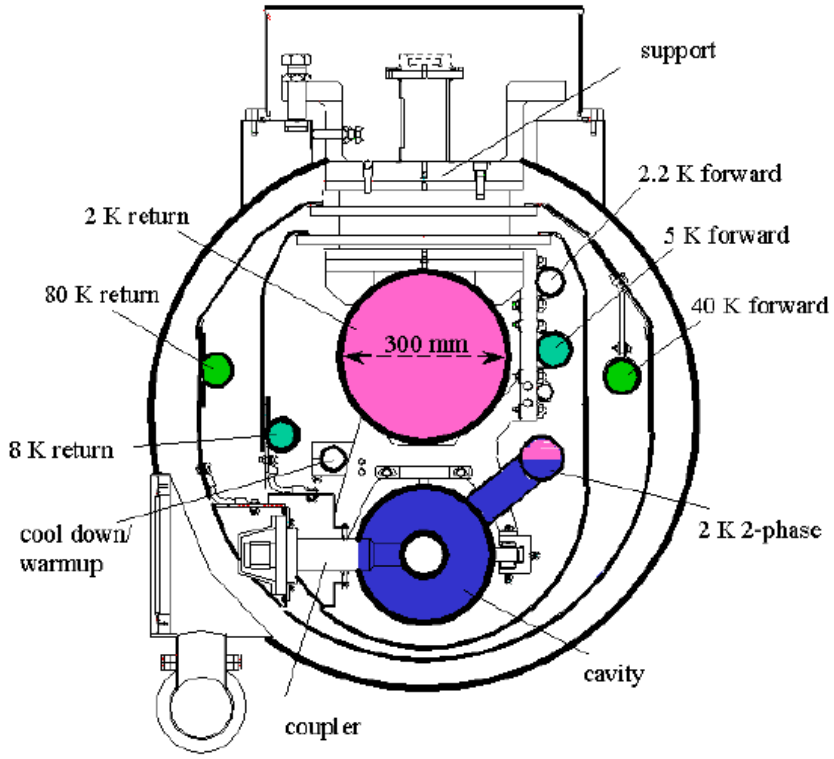


Figure 4: Cross section of a Tesla cryo-module [1]

very low losses are an important feature. The total heat load is then dominated by RF losses and the operational cost is in turn principally determined by cavity performances.

# 4 Parameters for the accelerating cavities and focusing magnets

The linac layouts have been optimized with the GenlinWin code [3]. The code simulates the motion of the synchronous particle thereby generating the longitudinal linac architecture. The optimization process considers several combinations of architectures taking into account independently-phase-tuned cavities of different length, energy transition between sections, number of cells and number of cavities per cryo-module. The study shows that a good option is to raise the beam energy from $50\ MeV$ to $2.5\ GeV$ through three different sections:

1. *a triple-spoke section* with triple-spoke cavities of $\beta_{opt} = 0.38$ working at a nominal accelerating gradient of $8\ MV/m$;

2. *a medium-$\beta$-elliptic section* with 5-cell-elliptical cavities of $\beta_{opt} = 0.61$ and $E_{acc} = 14\ MV/m$;

3. *a high-$\beta$-elliptic section* with 5-cell-elliptical cavities of $\beta_{opt} = 0.89$ and $E_{acc} = 20\ MV/m$.

Before presenting the general layout for both options, we want first to underline the technological choices assumed for the accelerating cavities and the quadrupole focusing magnets within the ESS.

## 4.1 Accelerating cavities

### 4.1.1 Spoke resonators

Since more than a decade, we observe a growing interest of many laboratories in developing spoke resonators within the framework of high power proton or ion accelerator projects. We can succinctly mention the EUROTRANS and EURISOL European studies [2] and the HINS US project [18]. A review of experimental and calculated RF data for spoke cavities is given in *Tab.* 1. Values of the accelerating gradients and the peak surface fields are given at $4.2\ K$ since no significant increase has been observed at $2\ K$ [14] for these parameters.

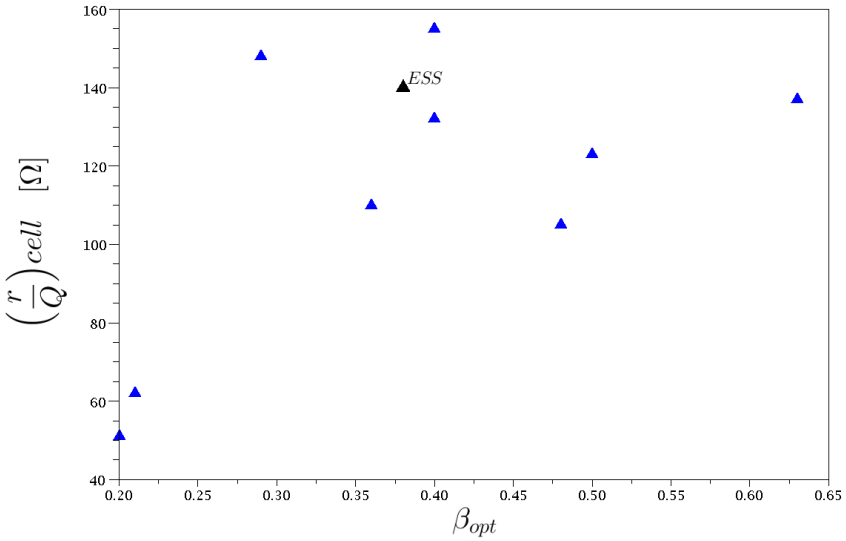


Figure 5: Ratios of the shunt impedance to the quality factor for one accelerating cell for spoke cavities as a function of the optimal beta

| **Labs** | $\beta_{opt}$ | Type | $E_{acc}$ $[MV/m]$ | $\frac{E_{pk}}{E_{acc}}$ | $\frac{B_{pk}}{E_{acc}}$ $[mT/(MV/m)]$ | $E_{pk}$ $[MV/m]$ | $B_{pk}$ $[mT]$ | $Q_0$ @ 4.2 $K$ | $Q_0$ @ 2 $K$ | $\left(\frac{r}{Q}\right)cell$ $[\Omega]$ | Ref. |
|---|---|---|---|---|---|---|---|---|---|---|---|
| IPN [1] | 0.20 | single | 4.77 | 6.74 | 14.48 | 32 | 69 | $1.2 \cdot 10^9$ | $6.3 \cdot 10^9$ | 51 | [10] |
| LANL [2] | 0.21 | single | 7.50 | 5.07 | 13.20 | 38 | 99 | $1.74 \cdot 10^9$ | $5 \cdot 10^9$ | 62 | [17, 16] |
| ANL [3] | 0.29 | single | 8.46 | 4.73 | 12.53 | 40 | 106 | $2.0 \cdot 10^9$ | $6 \cdot 10^9$ | 148 | [15, 14] |
| IPN | 0.36 | single | 8.15 | 4.66 | 12.76 | 38 | 104 | $8 \cdot 10^8$ | $2.5 \cdot 10^9$ | 110 | [9, 8] |
| ANL | 0.40 | single | 7.57 | 6.08 | 16.25 | 46 | 123 | $9.9 \cdot 10^8$ | $1.5 \cdot 10^9$ | 132 | [7] |
| ANL | 0.40 | double | 8.60 | 4.63 | 9.20 | 40 | 79 | $1.3 \cdot 10^9$ | [5] $4.2 \cdot 10^9$ | 155 | [4] |
| FZJ [4] | 0.48 | triple | 5.80 | 4.65 | 10.97 | 27 | 64 | $1 \cdot 10^9$ | $3 \cdot 10^9$ | 105 | [20] |
| ANL | 0.50 | triple | 7.65 | 3.72 | 11.47 | 28 | 88 | $2 \cdot 10^9$ | $7 \cdot 10^9$ | 123 | [11] |
| ANL | 0.63 | triple | 8.61 | 3.91 | 12.00 | 34 | 104 | $2 \cdot 10^9$ | $1 \cdot 10^{10}$ | 137 | [12] |

Table 1: Experimental and calculated RF data for spoke resonators



[1] Institut de Physique Nucléaire, CNRS/IN2P3-Université de Paris Sud, Orsay, France
[2] Los Alamos National Laboratory, Los Alamos, New Mexico, USA
[3] Argonne National Laboratory, Argonne, Illinois, USA
[4] Forschungzentrum, Jülich, Germany
[5] Calculated with an experimental residual resistance of 17 $n\Omega$

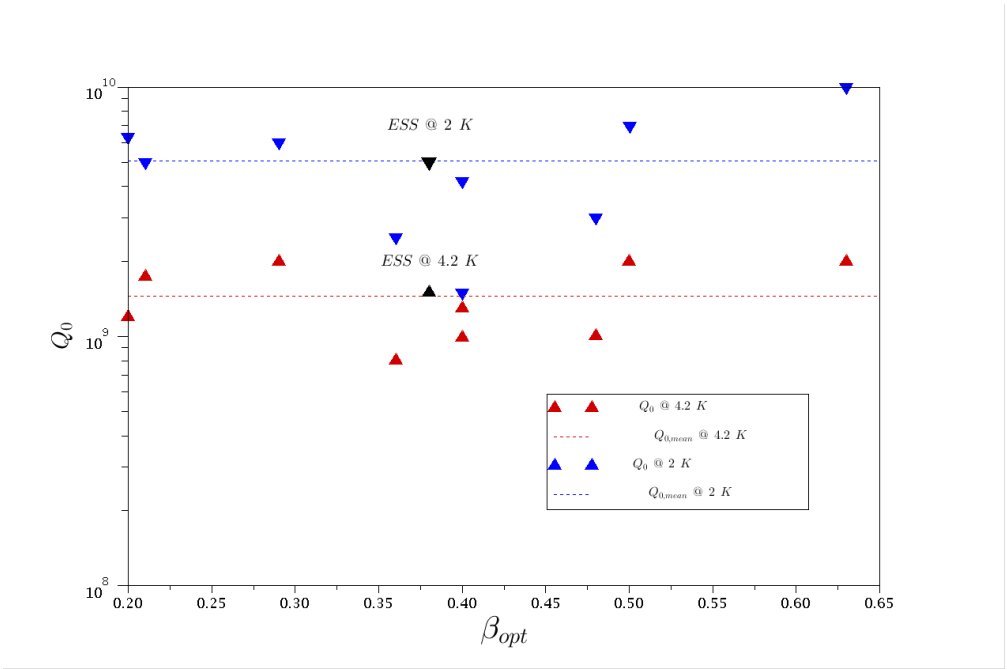


Figure 6: Quality factors for spoke cavities at low field as a function of the optimal beta

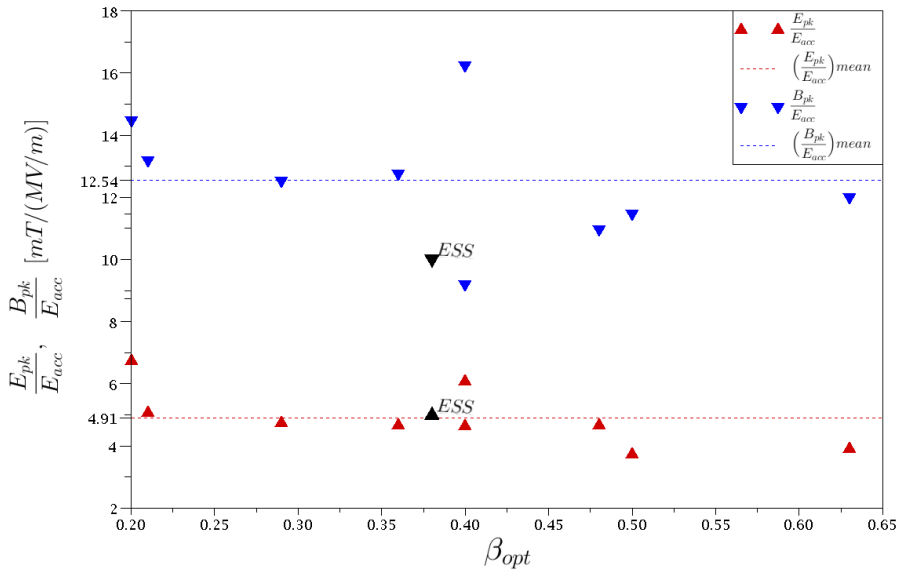


Figure 7: Ratios of the peak electric and magnetic fields to the accelerating gradient for spoke cavities as a function of the optimal beta

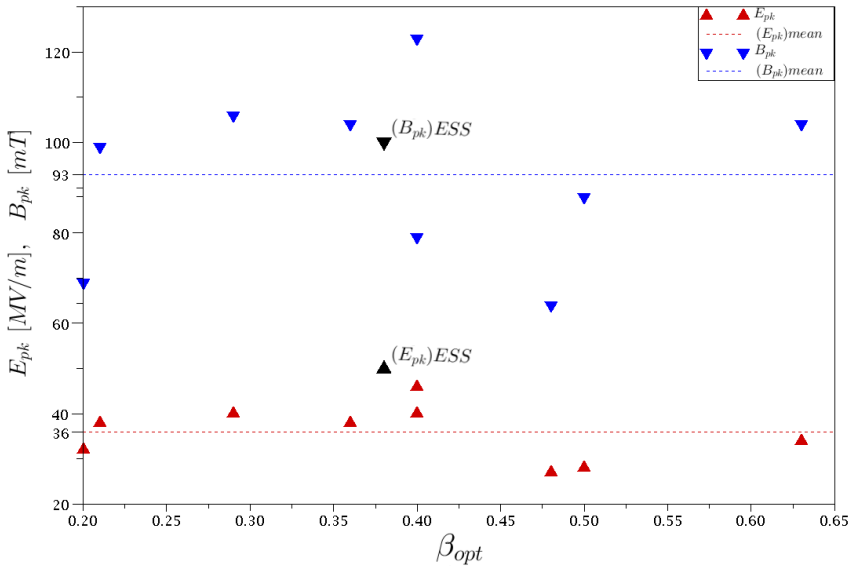


Figure 8: Ratios of peak surface electric and magnetic fields to the accelerating gradient for spoke cavities as a function of the optimal beta

*Fig.* 5 shows that the ratio of the shunt impedance to the quality factor $r/Q = 140\ \Omega$ for one accelerating cell corresponds to the upper values for spoke cavities. The quality factors at $4.2\ K$ and $2\ K$ fit the experimental average data plotted on *Fig.* 6. These two figures will be useful for the calculation of the dynamic RF heat load in section 6.

Concerning the ratio of the peak surface fields to the accelerating gradient, we can observe on *Fig.* 7 that $E_{pk}/E_{acc} \leq 5$ is commonly reached while designing spoke cavities with $B_{pk}/E_{acc} \leq 10\ mT/(MV/m)$ is more ambitious. However $B_{pk}/E_{acc} \leq 10\ mT/(MV/m)$ should become a standard value accordingly to the high level of cavity preparation techniques. On *Fig.* 8 are the peak electric and magnetic fields. We can see that $B_{pk} = 100\ mT$ has already been reached by almost half of the spoke cavities. On the contrary $E_{pk} = 50\ MV/m$ seems to be more challenging. Taking into account these latter parameters gives a maximal accelerating gradient of $10\ MV/m$. Thus, we have more than $20\ \%$ of safety margin on the nominal value of $8\ MV/M$.

According to the state-of-the-art of the spoke technology, we have chosen for the ESS triple-spoke cavity the parameters listed in *Tab.* 2.

From *Figs.* 5, 6, 7 and 8, we can mention as a general remark that spoke parameters do not seem to depend on the optimal beta. But there are few statistics on spoke cavities and more prototyping is necessary to bring an accurate conclusion.

| | |
|---|---|
| Frequency | $352.21\ MHz$ |
| Cell number | $4$ |
| Wall-to-wall length | $647\ mm$ |
| Optimal beta | $0.38$ |
| Maximum surface peak electric field | $50\ MV/m$ |
| Maximum surface peak magnetic field | $100\ mT$ |
| Cavity quality factor at $4.2\ K$ | $1.5 \cdot 10^9$ |
| at $2\ K$ | $5 \cdot 10^9$ |
| $r/Q$ | $560\ \Omega$ |
| Nominal accelerating gradient | $8\ MV/m$ |

Table 2: ESS triple-spoke cavity parameters

### 4.1.2 Elliptical cavities

We have followed the work already managed at CERN for the SPL and described in [5] to estimate the parameters of the elliptical cavities for the ESS. In *Tab.* 3 are listed the chosen parameters.

| | Medium-$\beta$ | High-$\beta$ |
|---|---|---|
| Frequency | $704.42\ MHz$ | |
| Cell number | $5$ | |
| All-cell length | $607\ mm$ | $894\ mm$ |
| Optimal beta | $0.61$ | $0.89$ |
| Maximum surface peak electric field | $50\ MV/m$ | |
| Maximum surface peak magnetic field | $100\ mT$ | |
| Cavity quality factor at $2\ K$ | $1 \cdot 10^{10}$ | |
| $r/Q$ | $224\ \Omega$ | $441\ \Omega$ |
| Nominal accelerating gradient | $14\ MV/m$ | $20\ MV/m$ |

Table 3: Parameters of the ESS elliptical cavities

## 4.2 Quadrupole focusing magnets

We assume a magnetic field value of $1\ T$ on pole tips for the normal conducting magnets of the segmented linac and a maximum value of $2\ T$ for the superconducting magnets of the not segmented linac with an aperture radius of $100\ mm$. The magnet lengths for both options are summarized in *Tab.* 4.

In the following section, we will see that a FDO scheme has been chosen for both designs. Between a focusing and a defocusing quadrupole magnets is a length of $300\ mm$.

| Section | Segmented design | Not segmented design |
|---|---|---|
| Triple-spoke | 250 | 125 |
| Medium-$\beta$-elliptic | 400 | 200 |
| High-$\beta$-elliptic | 400 | 200 |

Table 4: Length of the quadrupole focusing magnets (in $[mm]$)

A quadrupole package has then a length of $800\ mm$ for example in the triple-spoke section of the segmented design.

# 5 Presentation of the layouts

## 5.1 Lengths in the superconducting section of the ESS linac

Lengths in the superconducting section of the ESS linac meet realistic size requirements of cavity ancillaries and beam diagnostics along the propagation axis. Cavity ancillaries include higher order mode (HOM) damping filters, fundamental power couplers (FPCs), helium tanks and tuning systems. Beam diagnostics may be located inside the quadrupole package thanks to the $300\ mm$ free space. Wire scanners, beam position monitors and current transformers should form a beam diagnostics set. *Tabs.* 5 and 6 describes all the lengths taken into account for the simulations in the segmented design and the not segmented design respectively.

| | |
|---|---|
| Quadrupole package to cryo-module wall | 200 |
| Cryo-module wall to first cavity | 225 |
| Between cavities | 300 |
| Last cavity to cryo-module wall | 225 |
| Cryo-module wall to next quadrupole package | 300 |

Table 5: Lengths in a focusing period of the segmented linac (in $[mm]$)

| | |
|---|---|
| Cryo-module end to quadrupole package | 225 |
| Quadrupole package to first cavity | 300 |
| Between cavities | 300 |
| Between cryo-modules | [1] 0 |

Table 6: Lengths in a focusing period of the not segmented linac (in $[mm]$)

[1] At a first level of the study, we assume a null space between modules for the not segmented design

## 5.2 The segmented and not segmented designs

*Tabs.* 7 and 8 refers to the layouts and *Figs.* 9 and 10 shows a schematic view of the spoke and elliptic periods for the segmented and not segmented linacs respectively.

| Sections | Number of | | Lengths $[m]$ | | |
|---|---|---|---|---|---|
| | Cavities | Cryostats | Cryostat | Warm | Section |
| Triple-spoke | 21 | 7 | 3.02 | 1.30 | 30.23 |
| Medium-$\beta$-elliptic | 52 | 13 | 3.78 | 1.60 | 69.89 |
| High-$\beta$-elliptic | 128 | 16 | 9.70 | 1.60 | 180.80 |
| Total | 201 | 36 | | | $\sim 281$ |

Table 7: Layout of the segmented linac

| Sections | Number of | | Lengths $[m]$ | |
|---|---|---|---|---|
| | Cavities | Cryostats | Period | Section |
| Triple-spoke | 21 | 7 | 3.87 | 27.08 |
| Medium-$\beta$-elliptic | 52 | 13 | 4.78 | 62.09 |
| High-$\beta$-elliptic | 128 | 16 | 10.70 | 171.20 |
| Total | 201 | 36 | | $\sim 260$ |

Table 8: Layout of the not segmented linac

Avoiding space between modules yields a not segmented linac length of $260\ m$. The superconducting segmented linac is only $8\ \%$ longer with a length of $281\ m$. The difference can be estimate on the graphs of *Fig.* 12. Besides, even if the final energy is bigger at the end of the not segmented linac as can be seen in *Tab.* 9, *Figs.* 11 show that the real estate gradient is almost similar for both options.

| Sections | $W_{out}$ $[MeV]$ | |
|---|---|---|
| | Segmented | Not segmented |
| Triple-spoke | 139 | 141 |
| Medium-$\beta$-elliptic | 439 | 468 |
| High-$\beta$-elliptic | 2505 | [1] 2606 |

Table 9: Energy at the end of the sections for the segmented and not segmented linacs

[1] Phase lows have been chosen to be almost identical for both designs in order to have a consistent comparison but the phase low could be slightly changed in the not segmented design to readjust the final energy

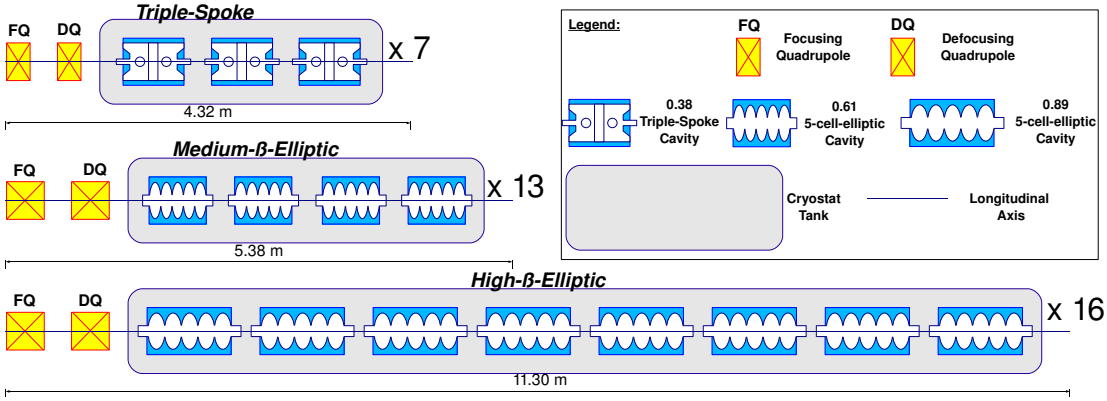


Figure 9: Schematic view of the segmented linac periods

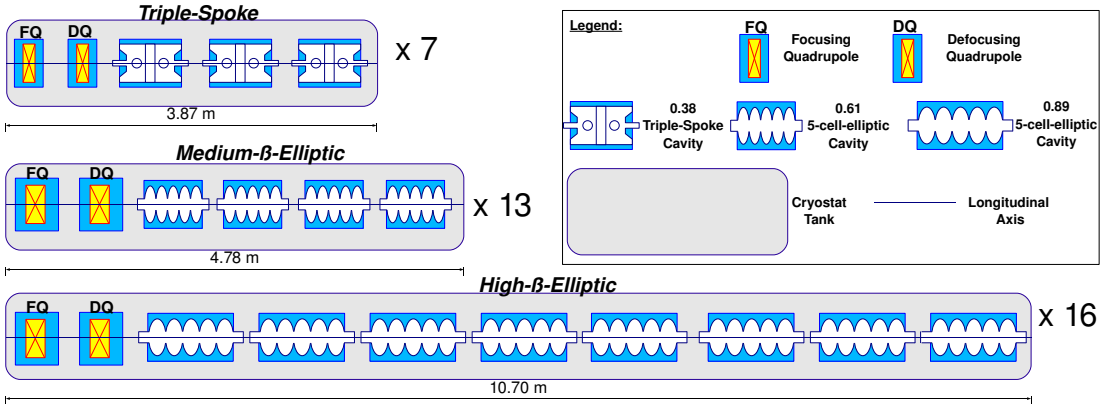


Figure 10: Schematic view of the not segmented linac periods

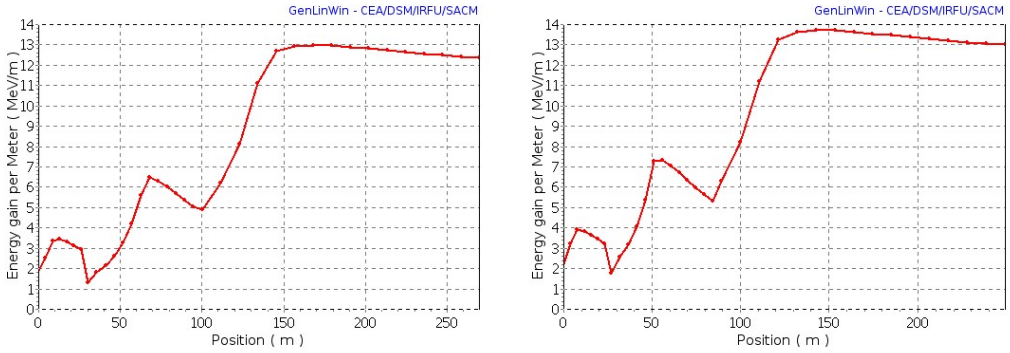


Figure 11: Energy gain per meter in the segmented (left) and not segmented (right) linacs

According to these preliminary observations, we can assess that the not segmented linac does not offer any significant advantage from the point of view of the total length and the real estate gradient for the ESS case.

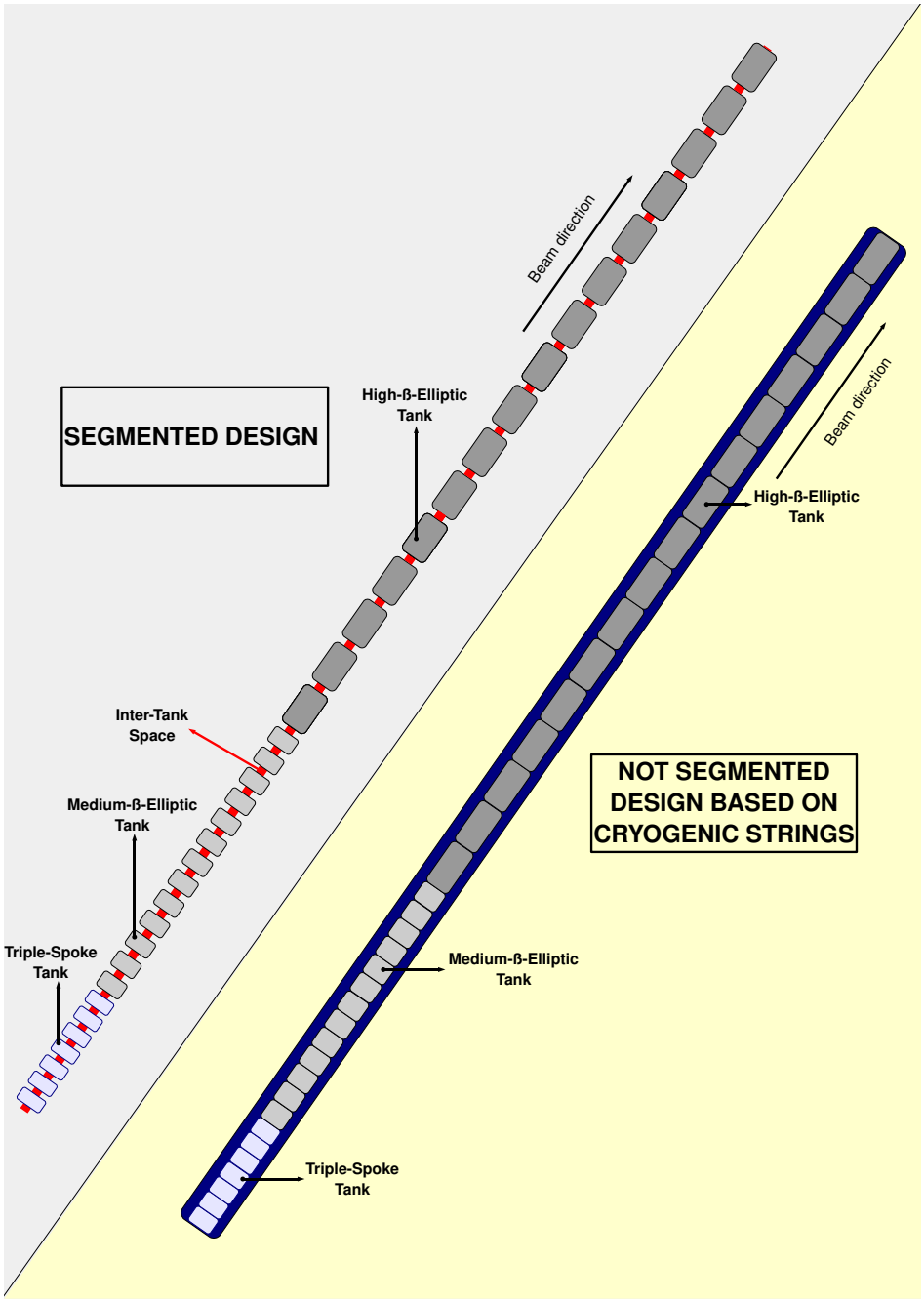


Figure 12: Schematic view of the segmented and not segmented linacs

# 6 Estimated heat loads

## 6.1 Method

The static load reported here for the segmented design are scaled from the measured values in the SNS modules [13]. They are estimated to be $1.9\ W$ per unit length of cavity with an additional contribution from the cold-to-warm transitions of $21.1\ W$ per module.

Concerning the not segmented design, values are taken from the estimated SPL module static losses [5] likewise scaled from the measured loads of the TTF modules [1] according to the higher surface and volume of the SPL cavities consequently fitting the ESS case. This gives $0.31\ W$ per unit length of cryo-module.

The dynamic RF load has been calculated using the cavity parameters reported in *Tabs.* 2 and 3. The RF power dissipation, $P_{diss}$, in the cavity walls is given by:

$$P_{diss} = \eta \frac{(E_{acc} L_{acc})^2}{\left(\frac{r}{Q}\right) Q_0} \tag{4}$$

where $\eta$ is the linac duty cycle. The quality factor drop from low field to the nominal gradient is ignored in the present study.

A rough estimation of the dynamic load contribution of $43\ \%$ of $P_{diss}$ from the FPCs ($3\ \%$) and HOM absorbers ($40\ \%$) is assumed [5, 1].

An additional contribution to the total losses for the not segmented design comes from the $5 - 8\ K$ level screening. Taking into account this contribution, it yields a static component of $1.33\ W$ per unit length of cryo-module. The dynamic component is assumed to be $23\ \%$ of the static loads at $5 - 8\ K$ for $4\ \%$ duty cycle.

Loss calculations in the $50 - 80\ K$ level thermal shielding are not presented in the study since losses at this temperature range have a negligible impact on the overall cryogenic budget.

## 6.2 Consideration of spoke $2\ K$ operation

Elliptical cavities must operate at $2\ K$ in sub-cooled liquid helium for stability and power consumption considerations. Thanks to a lower surface resistance at $352.2\ MHz$ and a geometry that leads to a relatively high mechanical robustness, operation at $4.2\ K$ in boiling helium is generally foreseen for spoke cavities. However high values of the quality factor at $2\ K$ could offset the additional cryogenic budget needed at this temperature.

Taking a ratio of $\epsilon_{4.2\ K}/\epsilon_{2\ K} = 3.5$ of the refrigerator efficiency at $4.2\ K$ to the refrigerator efficiency at $2\ K$ [6], we obtain the graphs presented on *Fig.* 13 giving the heat load in a spoke module for four different scenarios ($5 - 8\ K$ level contribution is not included). It means that we are considering that $1\ W$ lost at $2\ K$ is equivalent to $3.5\ W$ lost at $4.2\ K$.

The total load for the segmented design is largely dominated by the contribution of the static losses if a $4.2\ K$ operation is considered. This contribution becomes prohibitive when spoke cavities are cooled at $2\ K$.

Static and dynamic contributions are of the same order concerning the not segmented design at a $4\ \%$ duty cycle. However, the assumed $Q_0$ value at $2\ K$ is not enough to offset the additional cryogenic requirements needed to work at $2\ K$ even if they stay moderate.

It is meaningful from this preliminary study to consider a possible $2\ K$ operation for a spoke not segmented linac while the same working temperature for a segmented linac seems to be less significant due to very high induced losses in the cryogenic line.

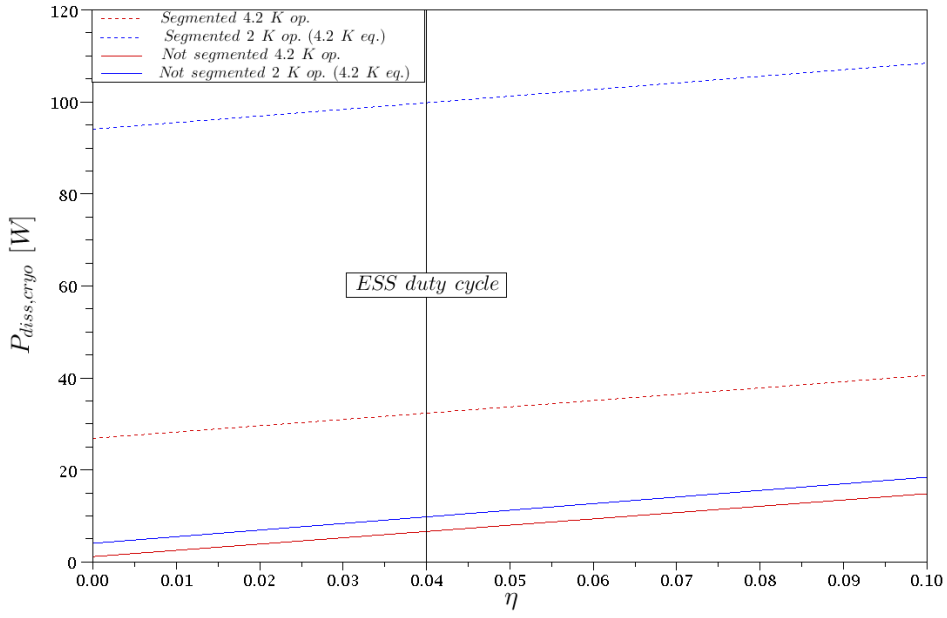


Figure 13: Estimated heat loads in the $4.2\ K$ and $2\ K$ cryogenic lines for a spoke module

## 6.3 Estimated heat load in the ESS linac

### 6.3.1 Presentation of the calculation results

In *Tab.* 10 are presented the calculation result of the estimated cryogenic load for the four different scenarios.

### 6.3.2 Analysis

The segmented design heat loads are largely dominated by static losses in the triple-spoke ($94$ % for $2$ $K$ operation and $82$ % for $4.2$ $K$ operation) and medium-$\beta$-elliptic sections ($75$ %). Equivalent static and dynamic contributions are, on the contrary, observed for the high-$\beta$-elliptic section ($48$ %).

Operating spoke cavities at $4.2$ $K$ yields a total cryogenic capacity of about $5.8$ $kW$. If $2$ $K$ spoke operation is considered, the triple-spoke section contribution raises from $3.7$ % to $10.4$ % adding $436$ $W$ to the total power consumption reaching then $6.2$ $kW$.

The dynamic RF losses play an important role in the total heat load of the not segmented design as compared to the segmented design. Static losses contribute only to $8$ % of the high-elliptic section and to $15$ % of medium-$\beta$-elliptic sections. However, we can observe that static and dynamic losses are of the same order in the triple-spoke section if $2$ $K$ operation is considered. In addition to the RF losses, we can observe that the intermediate shielding brings a significant contribution to the total losses. For example, almost half of the cryogenic power is required for the thermal shielding in the triple-spoke section.

The total power consumption is about $3.2$ $kW$. Operating spoke cavities at $2$ $K$ instead of $4.2$ $K$ adds a negligible contribution to the total cryogenic requirement.

The study also demonstrate that in the case of the ESS the segmented linac cryogenic consumption is $1.8$ and $1.95$ times on average the not segmented design consumption for $4.2$ $K$ and $2$ $K$ spoke operations respectively.

The beam loss should not surpass $1$ $W/m$. However, this limit increases substantially the total heat load of the not segmented linac to a bit more than $4$ $kW$ due to the wide superconducting length. Taking into account this additional load, the ratio of the segmented linac to the cryo-string-based linac total losses drops to $1.6$ and $1.7$ for $4.2$ $K$ and $2$ $K$ spoke operations respectively.

## 6.4 General comments about the validity of the calculations

The results presented in the study are always derived from experimental values of elliptical cavities at $2$ $K$. We estimate then that they give a realistic approximation for the

| | | Triple-spoke | Medium-$\beta$-elliptic | High-$\beta$-elliptic |
|---|---|---|---|---|
| Dynamic RF load per module $[W]$ | | (4.2 $K$ op.) 5.47<br>(2 $K$ op.) 1.64 | 8.43 | 37.30 |
| Static load per module $[W]$ | Segmented | 24.79 | 25.71 | 34.69 |
| | Not segmented | 1.20 | 1.48 | 3.32 |
| Static heat load contribution $[\%]$ | Segmented | (4.2 $K$ op.) 82<br>(2 $K$ op.) 94 | 75 | 48 |
| | Not segmented | (4.2 $K$ op.) 18<br>(2 $K$ op.) 42 | 15 | 8 |
| Heat load per module in the $5-8$ $K$ level shielding $[W]$ (only for the not segmented design) | | 6.33 | 7.82 | 17.50 |
| Contribution of the shielding to the total heat load $[\%]$ (only for the not segmented design) | | (4.2 $K$ op.) 49<br>(2 $K$ op.) 39 | 18 | 11 |
| Total heat load per module $[W]$ eq. at 4.2 $K$ | Segmented | (4.2 $K$ op.) 30.26<br>(2 $K$ op.) 92.51 | 119.49 | 251.97 |
| | Not segmented | (4.2 $K$ op.) 13.00<br>(2 $K$ op.) 16.27 | 42.51 | 159.67 |
| Total heat load per section $[kW]$ eq. at 4.2 $K$ | Segmented | (4.2 $K$ op.) 0.212<br>(2 $K$ op.) 0.648 | 1.553 | 4.032 |
| | Not segmented | (4.2 $K$ op.) 0.091<br>(2 $K$ op.) 0.114 | 0.553 | 2.555 |
| Total contribution per section $[\%]$ | Segmented | (4.2 $K$ op.) 3.7<br>(2 $K$ op.) 10.4 | 26.8<br>24.9 | 69.6<br>64.7 |
| | Not segmented | (4.2 $K$ op.) 2.8<br>(2 $K$ op.) 3.5 | 17.3<br>17.2 | 79.9<br>79.3 |
| Total heat load per linac $[kW]$ eq. at 4.2 $K$ | Segmented | (4.2 $K$ op.)<br>(2 $K$ op.) | 5.797<br>6.233 | |
| | Not segmented | (4.2 $K$ op.)<br>(2 $K$ op.) | 3.199<br>3.222 | |
| Total heat load per linac $[kW]$ eq. at 4.2 $K$ incl. 1 $W/m$ beam loss | Segmented | (4.2 $K$ op.)<br>(2 $K$ op.) | 6.533<br>7.022 | |
| | Not segmented | (4.2 $K$ op.)<br>(2 $K$ op.) | 4.043<br>4.133 | |

Table 10: Estimated heat load in the cryogenic lines assuming a $4\ \%$ duty cycle

ESS elliptic sections.

Concerning the spoke section, we have assumed the same method of approximation for the static loads as in the elliptic sections with no difference between both working temperatures ($4.2\ K$ and $2\ K$). Geometrical specificities between elliptical and spoke cavities have also been ignored. In addition to this first source of errors, the lack of statistics on spoke prototyping makes difficult the choice of the cavity parameters and leads consequently to decrease the accuracy of the RF dynamic loss calculations. The last point deals with the HOM damping filters. Spoke cavities are less subjected to HOM but no dedicated study has been performed until now. Taking into account the contribution ($40\ \%$ of the cavity contribution) of the HOM absorbers might have over-estimated the RF dynamic losses.

Regardless of the lack of accuracy of the calculations in the triple-spoke section, the general feature of the loss calculations is conserved. The order of magnitude of the figures of *Tab.* 10 allows the former conclusions to remain valid.

.

# 7 Conclusion

The study investigates two methods for cryostating based on proven technologies developed at the SNS and by the Tesla collaboration (applied now for the XFEL and ILC). A tunnel of $4.3\ m$ in width and $3.8\ m$ in height accommodates the SNS linac while the Tesla tunnel is a cylinder with a diameter of $5.2\ m$. After a general overview of the two concepts, parameter lists of the cavities, the quadrupole magnets and the main linac lengths are proposed for the ESS. The general linac layouts are then presented. The segmented and not segmented designs both include a triple-spoke section followed by a medium-$\beta$-elliptic section and a high-$\beta$-elliptic section. Losses are finally estimated for four different scenarios including or not including a spoke operation at $2\ K$.

The aim of a cryo-string-based linac design is a high real estate gradient with reduced cryogenic losses. The linac architecture is therefore more compact and the cryogenic line is surrounded by two levels of heat intercept shielding to minimize the static losses. The study shows that avoiding warm-to-cold transitions yields a not segmented design of $260\ m$. The segmented superconducting linac is only $8\ \%$ longer with a length of $281\ m$. Furthermore, the not segmented option does not offer a relevant advantage from the real estate gradient point of view.

While a $4.2\ K$ spoke operation seems better from the cryogenic point of view if a segmented linac is considered, it appears that a $2\ K$ spoke operation adds a negligible

supplement to the total not segmented linac losses. The study also reveals that the required cryogenic power for the segmented option ranges between $1.6$ and $1.7$ times the not segmented design needs. However, a segmented design-based linac permits replacement of a cryo-module in less than one day.

To sum up in a few words the main conclusions of the study, we have to highlight that:

1. the cryogenic consumption of the segmented linac is $1.6 - 1.7$ times the not segmented linac consumption;

2. operating spoke at $2\ K$ adds $7.5\ \%$ to the total heat load of the segmented linac with spoke resonators cooled at $4.2\ K$;

3. operating spoke at $2\ K$ in the not segmented design is almost transparent from the the cryogenics point of view.

The study does not give the contribution of the cryogenic cost as compared to the overall budget of the linac. However, if designing a fully segmented linac yields a significant increase, it would be interesting to design an "hybrid linac" with independent strings of $2$ or $3$ cryo-modules for instance thereby reducing the static loss contribution while keeping the possibility of rapid exchange.

# Acknowledgments

I acknowledge the valuable help of R. Duperrier for the reading of this paper and for his careful advise.

# References

[1] Tesla technical design report.

[2] J-L. Biarrotte. High power cw superconducting linacs for EURISOL and XADS. *Proceedings of LINAC'04, Lübeck, Germany*.

[3] R. Duperrier, N. Pichoff, and D. Uriot. CEA Saclay codes review. *ICSS 2002 conference, Amsterdam, The Netherlands*.

[4] J. D. Fuesrst et al. Superconducting $345\ MHz$ two-spoke cavity for RIA. *Proceedings of PAC'03, Standford, California, USA*.

[5] F. Gerick et al. Conceptual design of the SPL II: A high-power superconducting $H^-$ linac at CERN. *CERN-2006-006*.

[6] M. Kelly. Superconducting spoke cavities. *Proceedings of HB'06, Tsukuba, Japan*.

[7] M. P. Kelly. Cold test of a spoke cavity prototype for RIA. *Proceedings of PAC'01, Chicago, Illinois, USA*.

[8] G. Olry et al. Development of SRF spoke cavities for low and intermediate energy ion linacs. *Proceedings of SRF'03, Lübeck, Germany*.

[9] G. Olry et al. Recent developments on superconducting $\beta 0.35$ and $\beta 0.15$ spoke cavities at IPN for low and medium energy sections of proton linear accelerators. *Proceedings of EPAC'04, Lucerne, Switerland*.

[10] G. Olry et al. Development of spoke cavities for the EURISOL and EUROTRANS projects. *Physica C*, 2006.

[11] K. W. Shepard. Superconducting triple-spoke cavity for $\beta = 0.5$ ions. *Proceedings of PAC'05, Knoxville, Tennessee, USA*.

[12] K. W. Shepard et al. Prototype superconducting triple-spoke cavity for beta=0.63. *Proceedings of PAC'05, Knoxville, Tennessee, USA*.

[13] W. J. Shneider et al. Design of the SNS cryomodules. *PAC'01, Chicago, Illinois, USA*.

[14] T. Tajima. Consideration of $2\ K$ operation. *Workshop on the Advanced Design of Spoke Resonators, Los Alamos, New Mexico, USA*, 2002.

[15] T. Tajima et al. Evaluation and testing of a low-$\beta$ spoke resonator. *Proceedings of PAC'01, Chicago, Illinois, USA*.

[16] T. Tajima et al. Results of the two LANL $\beta = 0.175$, $350\ MHz$, 2-gap spoke cavities. *Proceedings of PAC'03, Standford, California, USA*.

[17] T. Tajima et al. Test results of the LANL $350\ MHz$, $\beta = 0.175$, 2-gap spoke resonator. *Proceedings of LINAC'02, Gyeongju, Korea*.

[18] R. C. Webber and G. Apollinari. Overview and status update of the Fermilab HINS linac R&D program. *Proceedings of PAC'09, Vancouver, British Colombia, Canada*.

[19] T. Whitlatch et al. Shipping and alignment for the SNS cryomodule. *PAC'01, Chicago, Illinois, USA*.

[20] E. Zaplatin et al. FZJ HIPPI SC triple-spoke cavity. *Proceedings of PAC'09, Vancouver, British Colombia, Canada*.